Corrsin lecture on hairy hydrodynamics

Invited Articles

Corrsin lecture on hairy hydrodynamics

A. E. Hosoi
Department of Mechanical Engineering and Department of Mathematics, Massachusetts Institute of Technology, Cambridge, Massachusetts 02139, USA

(Received 26 July 2019; published 18 November 2019)

Flexible slender structures in flow are everywhere. While a great deal is known about individual flexible fibers interacting with fluids, considerably less work has been done on fiber ensembles, such as fur or hair, in flow. These hairy surfaces are abundant in nature and perform multiple functions from thermal regulation to water harvesting to sensing. Motivated by these systems, I consider two examples of hairy surfaces interacting with flow which were presented in the Corrsin lecture at the 2018 APS-DFD meeting (71st Annual Meeting of the APS Division of Fluid Dynamics, Atlanta, 2018). In the first example I consider a toy problem of angled hairs in Couette flow. Using this simple model, I explore asymmetry in the flow and anomalous drag scaling by exploiting various limits in the parameter space. In the second example I consider viscous dipping, a feeding method utilized by many nectar drinking animals. Previous studies have analyzed these drinking strategies through the Landau-Levich-Derjaguin framework; however, many viscous dippers have hairy structures on their tongues that enhance fluid uptake. Here I investigate the impact of mesoscale hairy structures on feeding efficiency and conclude with general comments on drainage through beds of hairs.

DOI: 10.1103/PhysRevFluids.4.110508

I. INTRODUCTION

I have not had the good fortune to meet Stanley Corrsin, and having given the Corrsin lecture, I am quite certain that I missed out. Corrsin's remarkable accomplishments are of course well known and his intellectual impact on the fluid dynamics community is indisputable. What I previously failed to appreciate was the profound impact he has had on the lives of so many people in our community. Since receiving the Stanley Corrsin Award, I have been the recipient of a number of heartfelt correspondences from well-wishers; every one of those notes included a personal story or an anecdote about Stan which highlighted not only his brilliance, but his humor, his friendship, and his genuine care and support for his students and junior colleagues. The warmth of his personality shines through in multiple remembrances including the review by Phillips [1], who also noted the following: "Science begins, [Stan] would say, by asking simple questions about complex phenomena but advances by asking more penetrating questions about simpler systems, whose solution could be obtained with [rigor] and explained with clarity." That quote has inspired me to take a fresh look at our work on mesoscale structures interacting with flows and to focus this article on simple models that lend general insights into more complex phenomena. In the following I will attempt to strip away as much of the complexity from these systems as can be reasonably removed with the goal of extracting general optimization and design principles that may be relevant to both biological and engineered systems.

The broad theme of this work is ensembles of slender structures, i.e., hairs, interacting with flow. These interactions are ubiquitous in natural systems; they appear as wind through grass, as sensors in the inner ear and on the antennae of insects and crustaceans [2], as fur on diving marine mammals [3], and on the tongues of nectar-feeding organisms [4], to name a few. Several years

TABLE I. Overview of the hairy hydrodynamic systems we have investigated to date. Check marks indicate the dominant balances in the parameter regimes relevant to our experiments. Direction of flow indicates whether the fluid is moving primarily parallel to the hairs ∥ or perpendicular ⊥. Details of these studies appear in [3–6].

System	Viscosity	Gravity	Inertia	Elasticity	Capillarity	Flow direction	Analogous classical systems
	✓	✓				∥	dip coating
	✓	✓				⊥	draining films
	✓			✓		⊥	channel flow
	✓	✓	✓		✓	⊥, ∥	drop impact

ago, the pervasiveness of this recurring structure in nature inspired us to develop techniques for fabricating soft assemblies of hairs in which the geometric properties (hair length, diameter, spacing, etc.) could be precisely controlled (see the Supplemental Material in [3]). This ability to manufacture beds of flexible slender structures turned out to be a game changer for my laboratory; it pushed us to look at some of the most iconic fluid dynamic experiments in a new light and ask what happens when hairs or other mesoscale features are added to the boundaries. A summary of the systems we have investigated to date is presented in Table I, the details of which (along with experimental data) have appeared in previous publications. In the following I will take a closer look at two of these systems, channel flow and dip coating, and, in the spirit of Corrsin, dig into a few simple calculations that have not yet appeared in the literature.

II. FLEXIBLE HAIRS IN LOW-REYNOLDS-NUMBER CHANNEL FLOW

Although flows interacting with hairs are common in nature, our interest in hairs in channel flow began not with biology but with machine design and Tesla. In particular, we became interested in small-scale hydraulic systems which are comprised of a myriad of individual components, e.g., valves, pumps, throttles, etc.; Tesla noted that each of these components "... is a delicate contrivance, very liable to wear and get out of order and thereby imperil ponderous, complex and costly mechanisms" [7]. He then goes on to suggest that these shortcomings could be overcome if hydraulic components were designed as solid state elements, i.e., with no moving parts. This eventually led to his 1920 patent for a solid state valve, the valvular conduit, which offers asymmetric resistance to flow via decorating the channel with intricate lobes that preferentially draw fluid smoothly in one direction and dissipate energy in the other: "... the interior of the conduit is provided with enlargements, recesses, projections, baffles or buckets which, while offering virtually no resistance to the passage of the fluid in one direction, other than surface friction, constitute an almost impassable barrier to its flow in the opposite sense by reason of the more or less sudden expansions, contractions, deflections, reversals of direction, stops and starts and attendant rapidly succeeding transformations of the pressure and velocity energies" [7]. This remarkably clever concept relies on the inertia in the flow to break the directional symmetry in resistance; unfortunately, while this design may be effective at high Reynolds numbers, in a viscously dominated flow regime, no amount of complicated "enlargements, recesses, projections, baffles or buckets" will result in a directionally dependent flow owing to the time reversibility of Stokes flow.

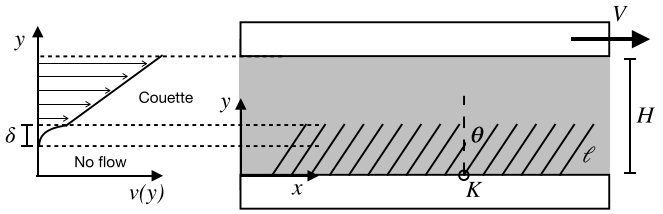

FIG. 1. Schematic of a toy problem to illustrate asymmetry induced by deformable hairs in channel flow. In the absence of flow, $\theta = \theta_S$.

A. Hairs in Couette flow

In order to carry this concept down to low Reynolds number, we require an additional effect to induce directional asymmetry. There are multiple ways this could potentially be achieved; one possibility is to trigger a flow-dependent geometric change in the channel which, in the spirit of this paper, can be achieved with deformable hairs. We begin by considering a simple bed of rigid hairs. In this system, deformation is achieved via torsional springs (of spring stiffness K) at the base of each hair which anchor the hairs to the substrate. The hairs are fixed at an angle θ_S (in the absence of flow) relative to vertical. To illustrate key concepts, we will investigate the response of this system when the bed of hairs is immersed in a Couette flow (see Fig. 1). Inspection of the schematic in Fig. 1 suggests that it is not unreasonable to expect to observe asymmetry: If the top plate is moved from left to right, the flow flattens the hairs, opening up the channel and reducing resistance to flow; in contrast, if the plate is moved from right to left, the hairs "stand up," obstructing the channel and increasing the flow resistance.

As a first-order estimate, we can model transport within the hair bed using a Darcy-Brinkman model given by

$$\nabla p + \frac{\mu}{k}\mathbf{u} = \mu_e \nabla^2 \mathbf{u}, \tag{1}$$

where p is pressure, μ is the dynamic viscosity of the fluid, μ_e is the so-called effective viscosity associated with the Brinkman term, $\mathbf{u}$ is the velocity field, and k is the permeability of the bed. In a long slender channel, at low Reynolds number, we expect the flow profile to resemble that sketched in Fig. 1, in which there is no flow near the base of the bed and the velocity profile is linear in the open channel above the hairs. These two regions are connected via a boundary layer that penetrates a depth δ into the bed of hairs. At this point, it is instructive to estimate the size of this connecting boundary region δ in the hopes of perhaps further simplifying our calculation in certain limits. Since there is no pressure gradient in Couette flow, the last two terms in Eq. (1) must balance, implying $\mu V/\delta^2 \sim \mu_e V/k$. Hence the thickness of the boundary region scales as $\delta \sim \sqrt{\mu_e k/\mu}$.

This length scale δ can be compared to the length of the hairs ℓ to estimate the fraction of the bed occupied by the boundary layer. Such a comparison suggests two potentially interesting limits: one in which the boundary layer fills the entire hair bed and one in which it is negligibly small. While both of these limits are worth investigating, I will focus on values of δ/ℓ that are most relevant to the biological and synthetic cases discussed herein. In particular, in this paper we largely focus on systems with dense arrays of hairs; in that limit, Gopinath and Mahadevan [8] have shown that the permeability can be approximated as $k \approx a^2(1-\phi_s)^2/4\phi_s$, where a is the radius of the individual hairs and ϕ_s is the area fraction occupied by the hairs. Hence, in the dense hair limit, the fraction of the bed occupied by the boundary region can be approximated as

$$\frac{\delta}{\ell} \approx \frac{a(1-\phi_s)}{2\ell\phi_s^{1/2}}\left(\frac{\mu_e}{\mu}\right)^{1/2}. \tag{2}$$

In our systems $a/\ell < 0.1$ and values in the literature for μ_e/μ range between 1 and 10 [9]. Hence δ is at least an order of magnitude smaller than ℓ provided $\phi_s \gtrsim 0.5$ (as is the case in our systems). Since $\delta/\ell \ll 1$ we can make two helpful simplifying approximations. First, since the thickness of the boundary layer is much smaller than the length of the hairs, we can approximate the fluid force acting on the hairs as a concentrated force applied at the tip of each hair. Second, since the bulk of the flow occurs in the upper clear portion of the channel, to lowest order we can estimate the fluid flux as that given by Couette flow in the upper (nonhairy) portion of the channel.

Given these two approximations, the flow profile in the x direction in the unobstructed portion of the channel is given by $v(y) = Vy/G(\theta)$, where V is the velocity of the top plate, θ is the equilibrium angle of the hairs when the plate is moving, and the gap G between the tip of the hairs and the top plate is given by $G = H - \ell\cos\theta$; the channel height H and the hair length ℓ are shown in Fig. 1. The equilibrium angle of hairs θ is set by a torque balance between the torsional spring at the base of each fiber and the shear stress acting at the tip. To estimate the applied moment at the fiber tips, we assume that the shear stress $\tau = \mu V/G$ is completely supported by hairs.[1] The torque balance can then be written as

$$\frac{\mu V}{H - \ell\cos\theta}\frac{\pi a^2}{\phi_S}\ell\cos\theta + K(\theta_S - \theta) = 0. \tag{3}$$

Rearranging Eq. (3) reveals two relevant dimensionless quantities: the ratio of the hair length to the channel height $\alpha \equiv \ell/H$ and the ratio of the characteristic force arising from the torsional spring to the characteristic viscous forces acting on the hairs $\beta \equiv K\phi_S/\mu V a^2$. These can be incorporated to express (3) in its dimensionless form

$$\frac{\pi\alpha\cos\theta}{1 - \alpha\cos\theta} + \beta(\theta_S - \theta) = 0. \tag{4}$$

Equation (4) is a transcendental equation for the equilibrium angle of the hairs θ which can be solved numerically. Returning to Tesla, we are reminded that the valve efficacy "... is chiefly determined; [*sic*] first, by the magnitude of the ratio of the two resistances offered." This ratio can be captured by computing the ratio of the flux to the right $Q_R = VG/2 = \frac{V}{2}(H - \ell\cos\theta)$ to the similarly computed flux to the left Q_L,

$$R = \frac{1 - \alpha\cos\theta_R}{1 - \alpha\cos\theta_L}, \tag{5}$$

where θ_R is equilibrium configuration of the hairs when flow goes from left to right and θ_L is the equilibrium configuration with flow in the opposite direction.

The design space of our toy "valve" can now be parametrized by three dimensionless groups: the geometric ratio of channel height to hair length α, the dynamic ratio of spring forces to viscous forces β, and the equilibrium angle of the hairs with no flow θ_S. In Fig. 2 we show two slices through this space: one at fixed $\alpha = 0.7$ and one at fixed $\theta_S = \pi/2$. There are several features in this design space that are worth emphasizing. First, consider Fig. 2(a). In the limit of small θ_S, each fiber is nearly vertical. If the fiber is vertical, the deformation under flow to the right is the mirror image of the deformation under flow to the left, and therefore $R \to 1$ (i.e., there is almost no asymmetry). Second, in the small β limit, the torsional spring is very soft relative to viscous forces. Hence each fiber lies nearly flat against the channel wall regardless of flow direction, and again there is no asymmetry, $R \to 1$. Finally, in the large β limit, the torsional spring is very stiff and the viscous stresses are insufficient to impart a significant change in the hair orientation when flow is turned on in either direction. Recall that at low Reynolds numbers, if the hairs do not change configuration

[1]The distribution of the load between hairs and fluid is discussed in the Appendix, where we find, for the systems under consideration in this paper, that the bulk of the load is carried by the hairs.

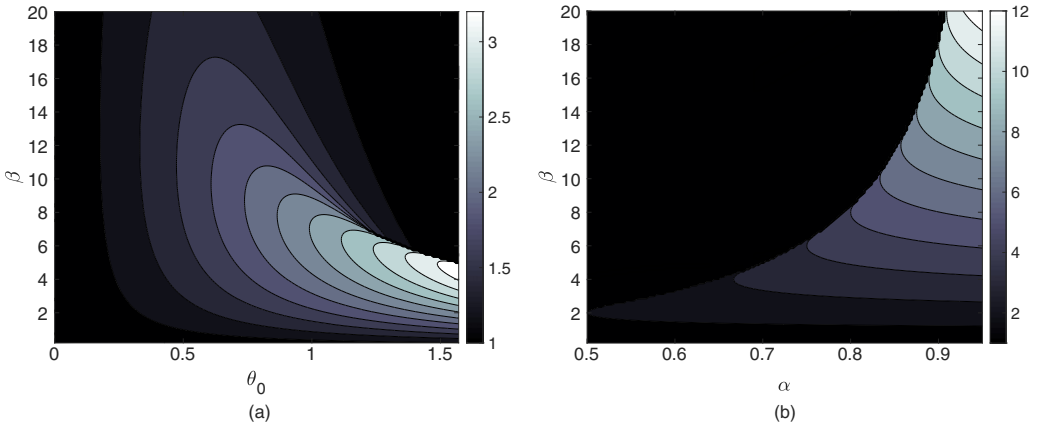

FIG. 2. (a) Flow ratio R for a fixed ratio of channel height to hair length $\alpha = 0.7$. (b) Flow ratio R at fixed $\theta_S = \pi/2$. Color indicates R with black indicating no asymmetry in the flow.

with flow direction, time reversal symmetry dictates that the local velocity profiles are mirror images of one another when the flow direction is reversed and again $R \to 1$.

However, at large θ_S and at intermediate values of β where spring and viscous forces are comparable, asymmetry emerges. As one might expect, the asymmetry is maximized as $\theta_S \to \pi/2$ and $\alpha \to 1$. Setting $\theta_S = \pi/2$, we now consider a slice in the α-β plane [Fig. 2(b)] and find that the optimal spring stiffness increases as the fraction of the channel occupied by the hairs increases. This is again intuitively consistent since for fixed V, the maximum shear stress experienced by the fibers increases as the gap decreases. As a side note, it appears that for a given α and θ_S, the asymmetry drops precipitously when β exceeds a critical value. This seems to indicate that if there is some uncertainty in the design it is far better to err on the side of selecting a β below the optimal value rather than above.

B. Reconfiguration and anomalous drag scaling

The fundamental concept of a velocity-dependent resistance to flow that is illustrated in this simple toy problem is a recurring theme in the biological literature. It often appears under the guise of reconfiguration or anomalous drag scaling, perhaps most famously in the works of Koehl [10] and Vogel [11,12], who have performed extensive studies on wind and water loading on sessile organisms (e.g., [10–12]); in the words of Koehl, "... standing in one place is not as simple as it may at first seem ..." [10]. Both Vogel and Koehl note that there is almost always a compromise associated with standing still in flow. On the one hand, organisms should reduce their cross-sectional area to minimize drag and hence minimize internal mechanical stresses which increase the risk of damage. On the other hand, many of these organisms rely on large surface areas to collect nutrients, gain exposure to sunlight, transport gases, etc.

The observed solution for many organisms is a finely tuned geometry that leverages flexibility as flow speed increases: "Shape becomes a function of speed ..." [11]. For example, in trees there is a trade-off between exposing a large leaf surface area to sun and the danger of blowing the tree over during periods of high wind. Simply adding flexibility to the leaves without taking into account geometric considerations is not necessarily helpful; recall that the drag on a flapping flag *increases* relative to its rigid counterpart, hence adding flexibility to leaves such that they act as flapping flags would be an unmitigated disaster. However, tree leaves avoid this pitfall by rolling into a conical configuration in high wind (rather than flapping), reducing their effective cross-sectional area: "Instead of being a pure liability, as in a flag, flexibility is at least in part a virtue in the upper portions of a tree" [12]. The available biological measurements suggest that appropriately structured reconfiguration leads to a reduction in the velocity exponent in the traditional drag scaling laws,

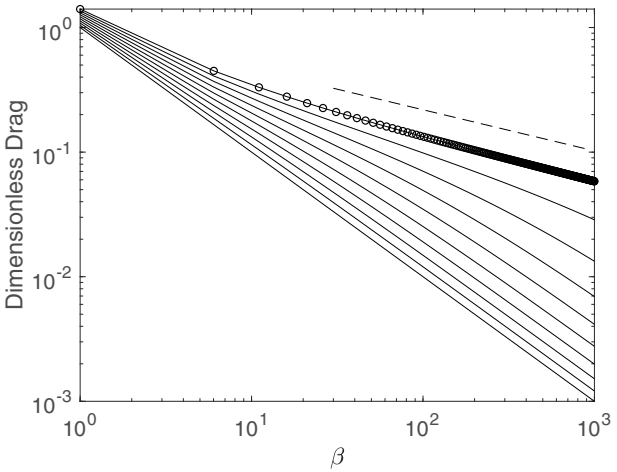

FIG. 3. Dimensionless drag as a function of $\beta \sim 1/V$. The dashed line indicates a slope of $1/3$. Solid lines indicate different values of θ_S with the topmost (highlighted by circles) $\theta_S = 0$. In all calculations $\alpha = 0.999$.

namely, the effective drag force scales like $D \sim V^{2-E}$, where E is a measure of the deviation from the standard high-Reynolds-number drag scaling.

Given the importance of anomalous drag scaling in biological systems, we return to our toy model to determine whether insights can be gleaned in computing E for our simple hairy Couette cell. In this case, E is defined as the deviation from the expected drag scaling at low Reynolds number, namely, $D \sim V^{1-E}$. We begin by estimating the drag force on the hair bed in the potentially interesting regime where $\alpha \to 1$ and $\beta \equiv 1/\epsilon \gg 1$, which reflects the small velocity, small deflection limit; to simplify the calculation, we will take $\theta_S = 0$. In these limits, Eq. (4) becomes

$$\epsilon\pi \cos\theta - \theta(1 - \cos\theta) = 0, \tag{6}$$

which we can solve order by order by expanding θ in powers of ϵ, namely, $\theta = \theta_0 + \epsilon^n\theta_1 + \epsilon^{2n}\theta_2 + \cdots$. The zeroth-order balance yields $\theta_0 = 0$, as expected in the low velocity limit. After some algebra, the next-order correction yields $n = 1/3$ and $\theta_1 = (2\pi)^{1/3}$. Hence, to leading order

$$\theta = \left(\frac{2\pi}{\beta}\right)^{1/3} + \cdots = \left(\frac{2\pi\mu V a^2}{K\phi}\right)^{1/3} + \cdots .$$

To calculate the drag anomaly E, we first write the drag force acting on the hair bed as $D = \tau A = \mu V A/(H - \ell\cos\theta)$. Rescaling D by $K\phi A/Ha^2$ yields the dimensionless form of the drag force: $D^* = [\beta(1 - \alpha\cos\theta)]^{-1}$. Substituting the leading-order term for θ into this expression, we find

$$D^* = \frac{2}{(2\pi)^{2/3}\beta^{1/3}}. \tag{7}$$

Since $\beta \sim 1/V$ the drag scales as $V^{1/3}$. At low Reynolds number, the expected scaling is linear in V, and hence the correction to the classical drag law is $E = 2/3$. A comparison of this scaling prediction with the drag obtained via the full solution to Eq. (6) is shown in Fig. 3.

Coincidentally, this correction is the same value found by Shelley and Zhang in their work on the drag on flexible beams in soap films, which represents another iconic chapter in the book of reconfiguration. In that case, the scaling arises from a characteristic length scale that reflects the effective cross-sectional area of the bending fiber, $L_0 \sim V^{2/3}$; this leads to a drag scaling of $V^{4/3}$, which was observed in both experiments and numerical simulations. (The fact that $E = 2/3$ in

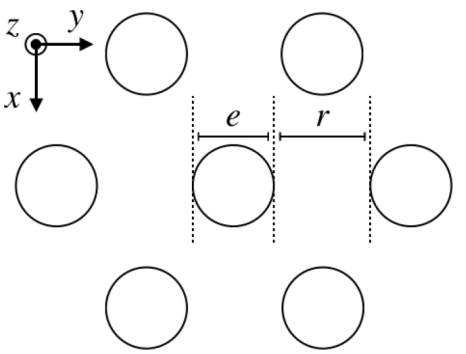

FIG. 4. Schematic of hair geometry in draining films. Circles represent hair cross sections. Gravity points in the x direction.

both systems appears to be completely fortuitous given that the two approaches apply to different Reynolds-number regimes and use different models for elasticity.)

C. Hairs in Poiseuille flow

It is straightforward to extend our analysis of hairs in Couette flow to hairs in Poiseuille flow with the added twist that we can no longer neglect the flow inside the bed of hairs. Instead, as a first-order estimate, one can patch together Poiseuille flow in the hairless central region of the channel with flow inside the hair bed given by Darcy (or Darcy-Brinkman) flow. The full derivation of Q is not dramatically different from the Couette case and is left as an exercise for the reader. However, I felt it was appropriate to mention the pressure-driven case because the identical approach was taken over 40 year ago to investigate another biological system by none other than Stanley Corrsin and collaborators [13]. In this work Erian, Corrsin, and Davis investigate placental blood flow and model the complex network of capillaries and so-called villous tree as an effective medium with a velocity-dependent permeability: another beautiful example of the functional coupling of velocity and shape in biology.

III. BATS AND OTHER NECTARIVORES

The second system I will highlight here was inspired by drinking bats. It is known that the tongues of bats and a number of other nectarivores are covered in small hairs, and it has been hypothesized that these hairs may play a functional role in enhancing nectar uptake. In this case our model system is a hairy plate withdrawn from a bath of viscous fluid. At first glance this appears to be analogous to the Landau-Levich-Derjaguin (LLD) dip coating problem [14,15]; however, a simple order-of-magnitude estimate reveals that surface tension does not play an important role at scales relevant to bats, hence the dominant physical effects are quite different from those of classical LLD when hairs are in play. Laboratory experiments to measure fluid uptake reveal two competing effects that predominantly determine the amount of fluid withdrawn by the plate: On the one hand, increasing the density of hairs slows the rate of drainage off the "tongue," so in principle more fluid can be transported to the throat of the nectarivore; on the other hand, more hairs also take up precious real estate on the tongue that could be used to carry more nectar. The optimal hair spacing is set by a balance between these two effects; details of this calculation appear in [4] and I will briefly outline a portion of the derivation here to lay the groundwork for the following discussion.

To estimate the amount of fluid lost to drainage, we begin with Stokes flow through a bed of hairs where the geometry is shown in Fig. 4:

$$\nabla p = \mu \nabla^2 \mathbf{v} + \rho \mathbf{g}. \tag{8}$$

Here **g** is gravity and the other quantities remain as defined above. To reduce the dimensionality of the model, we make an ansatz that flow is primarily confined to virtual "channels" between hairs and that flow in the direction of drainage can be reasonably approximated as parabolic in y on the scale of the hair spacing. Substituting this ansatz into (8) yields a two-dimensional (2D) Brinkman-like equation in which the hairs are essentially acting as a porous medium. Finally, we exploit the fact that characteristic length scales in z are much smaller than characteristic length scales in x; we apply a lubrication approximation to the 2D Brinkman equation, which results in the ordinary differential equation for the velocity profile (see [4] for details)

$$\mu\left(\frac{\partial^2 v}{\partial z^2} - \frac{12}{r^2}v\right) = -\rho g, \tag{9}$$

where $v(z)$ is the component of the fluid velocity in the direction of drainage (x direction) and r is the spacing between hairs. Solving for $v(z)$, we find

$$\frac{v(z)}{V_{\text{drain}}} = 1 - \cosh\left(\frac{2\sqrt{3}(\ell - z)}{r}\right)\text{sech}\left(\frac{2\sqrt{3}\ell}{r}\right), \tag{10}$$

where the characteristic drainage velocity is given by $V_{\text{drain}} = \rho g r^2/12\mu$. We will return to this expression for $v(z)$ in the upcoming derivation of the evolution of a draining film, but first we will simply make use of the characteristic drainage velocity to connect back to nectarivores.

To estimate the amount of fluid withdrawn by the tongue, we assume that the hair bed is initially filled with fluid; the amount of fluid that ultimately makes it to the bird's throat can be approximated using the total volume available for nectar in the absence of hairs (namely, the surface area of the tongue times the length of the hairs) and subtracting the volume occupied by hairs and the fluid lost to drainage. In addition, we make this quantity dimensionless by normalizing by total volume available. This leads to the following expression for the amount of fluid drawn up by the tongue, where asterisks indicate rescaled dimensionless quantities:

$$M^*(e^*, r^*) = \left[1 - \frac{\pi}{6\sqrt{3}}\frac{e^{*2}}{(e^* + r^*)^2}\right](1 - r^{*2}). \tag{11}$$

Here the second term in the square brackets represents volume exclusion by the hairs and the $(1 - r^2)$ represents drainage. All lengths, e^* and r^*, have been nondimensionalized by $r_0 = \sqrt{12\mu V/\rho g}$. Equation (11) reflects the total volume of nectar that the organism can capture as a function of hair radius and hair spacing; this function is plotted in Fig. 5. As with our hairy channel flow design space, there are a few interesting features in this landscape worthy of discussion. First, the amount of nectar taken up is maximized at the left edge of the plot. This suggests that in an ideal world, the tongues of nectarivores would all be covered in infinitesimally thin hairs which impede flow without taking up any space ($e^* \to 0$). Clearly this is not feasible as there are limits to how thin biological structures can be and still withstand the rigors of everyday life. Hence, rather than asking where uptake is maximized, a more sensible question to ask is, given an achievable hair radius e^*, what is the ideal spacing of the hairs? The answer to this question is shown as the dashed line in Fig. 5 (dotted lines show the region in which the fluid uptake is within 99% of this ideal spacing).

Finally, in the figure we have included values of hair diameter and hair spacing reported in the literature for four species of nectarivore: *Glossophaga soricina* (bats), *Trichoglossus moluccanus* (rainbow lorikeet), *Tarsipes rostratus* (honey possum), and *Apis mellifera ligustica* (honey bee). All but the honey bee lie within the 99% tolerance region of the hair spacing value that maximizes nectar uptake in our simple model. In hindsight, it is perhaps not surprising that the honey bee is an outlier; bees are considerably smaller than the other organisms represented here and hence our original assumption that surface tension can be neglected may no longer be valid.

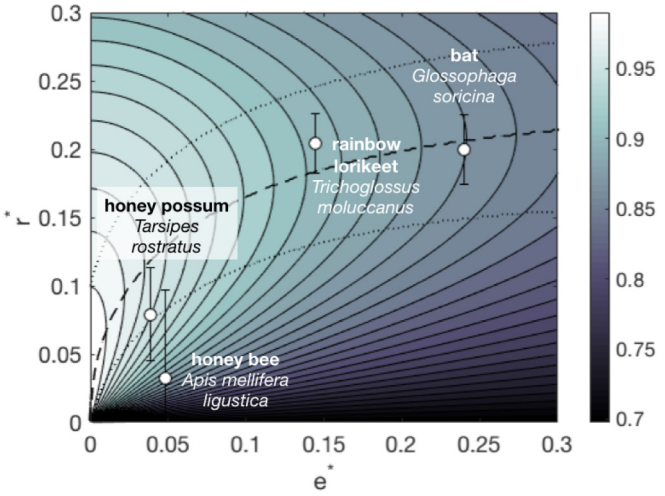

FIG. 5. Fluid uptake as a function of dimensionless hair diameter e^* and dimensionless hair spacing r^*. Color corresponds to dimensionless volume of fluid captured. The dashed line indicates the optimal spacing for a given hair radius e^*; dotted lines indicate the region in which the fluid uptake is within 99% of the maximum value. White points indicate measured values of hair diameter and spacing for different species taken from the literature.

Hairs and draining films

While Fig. 5 provides a reasonably satisfactory picture regarding the spacing of hairs on bat tongues, the analysis reveals a number of unresolved fundamental fluid dynamics questions. Shifting our attention away from bats and returning to the canonical problem of a viscous fluid draining through a bed of hairs, we can combine the velocity profile derived in Eq. (10) with mass conservation and write down an equation for the evolving shape of the free surface of a thin film draining through a bed of hairs:

$$\frac{\partial h}{\partial t} + V_{\text{drain}} \frac{\partial}{\partial x}\left[h - \frac{r}{2\sqrt{3}} \tanh\left(\frac{2\sqrt{3}h}{r} \right) \right] = 0. \tag{12}$$

Given this expression, there are a multitude of interesting questions we can tackle, analogous to those addressed in the context of draining films on smooth plates (e.g., stability, front propagation, fingering, undercompressive shocks, etc.). For starters, I will present just the tip of the iceberg here and explore two limits of this evolution equation: sparse and dense hair spacing.

First, consider dense hair spacing $h/r \gg 1$. In this limit $\tanh(2\sqrt{3}h/r) \approx 1$; hence the second term in the square brackets in Eq. (12) can be neglected relative to the first and the evolution equation becomes a linear first-order wave equation with propagation speed V_{drain}:

$$\frac{\partial h}{\partial t} + V_{\text{drain}} \frac{\partial h}{\partial x} = 0.$$

This is the appropriate limit for the bat tongue analysis; hence using V_{drain} to estimate the rate of drainage without computing the details of the film profile as governed by Eq. (12) is likely to be an acceptable approximation.

The sparse hair limit $h/r \ll 1$ is perhaps mathematically more interesting; this calculation was suggested to me by Howard Stone after I gave the Corrsin lecture at the APS-DFD meeting and who moreover provided a sketch of the solution on a napkin. Expanding on the cocktail napkin

calculation, in the sparse limit we expand $\tanh x = x - x^3/3 + 2x^5/15 + \cdots$ and Eq. (12) becomes

$$\frac{\partial h}{\partial t} + \frac{\rho g}{3\mu}\frac{\partial}{\partial x}\left[h^3\left(1 - \frac{24}{5}\frac{h^2}{r^2} + \cdots\right)\right] = 0. \tag{13}$$

At lowest order, the $(h/r)^2$ term can be neglected and the remaining two terms constitute Jeffreys' equation for a draining thin film on a vertical plate [16]. The similarity solution $h(x,t) = (\mu x/\rho g t)^{1/2}$ in this limit is well known and follows a thinning law in which $h \sim 1/\sqrt{t}$. Note that this solution does not contain r or any parameters associated with the hairs; it merely reflects the fact that, in the limit that the density of hairs goes to zero, we recover the flat plate solution. To obtain the first-order correction term due to the hairs, we can rescale h by ℓ and and define $\epsilon = \ell/r \ll 1$. We then expand this dimensionless h in powers of epsilon, $h(x,t) = h_0(x,t) + \epsilon^2 h_1(x,t) + \cdots$, where $h_0(x,t)$ is the Jeffreys similarity solution. This yields an inhomogeneous, variable coefficient, linear, first-order wave equation for h_1 which can be solved via a combination of integrating factors and the method of characteristics. Comparison of this solution with experimental data is beyond the scope of the present work.

IV. CONCLUSION

Finally, I would like to conclude by listing the three biggest lessons that I will take away from my Corrsin lecture experience. First, a wealth of interesting fluid dynamics appears when classical experiments are combined with mesoscopic modifications of boundaries: pick your favorite fluid dynamics experiment and add hairs! Second, hearing from Stanley Corrsin's many students, colleagues, and friends reminded me that our best scientific contributions are amplified through the personal connections we develop and foster throughout our careers. And last but not least, when someone hands you a napkin with equations at the APS-DFD meeting, save the napkin.

ACKNOWLEDGMENTS

First and foremost I would like to acknowledge the students and postdocs whose diligence and insights solved all of our hairy problems, in particular, Jean Comtet, who performed all of the initial calculations on deformable hair beds and had the insight to consider rigid rods on torsional springs; José Alvarado, who figured out how to manufacture the hairy surfaces which are foundational to all of the work herein; Alice Nasto, who spearheaded the work on bats and other organisms (for more on hairs, fluids, and biology, see Ref. [17]); and P.-T. Brun, who led the work on draining thin films including proposing both the original ansatz to reduce the dimensionality of the system and the key idea to consider the general problem of Brinkman flows in the lubrication limit. In addition, I would like to thank Alejandro Rico-Guevara for teaching us about rainbow lorikeets and sharing his lorikeet data and Howard Stone for suggesting that the sparse limit of the drainage evolution equation may be interesting, particularly as it relates to Jeffreys' equation. Finally, I would like to thank everyone who reached out and shared their delightful stories about Stan. This work was partially supported by the US Army Research Office under Grant No. W911NF1510166.

APPENDIX: LOAD DISTRIBUTION AT THE INTERFACE

In general, load distribution between the solid and fluid phases at the boundaries of porous media remains an open question. In the following I present an estimate to argue that, in our systems which lie in the parameter region of dense hair beds and low-Reynolds-number flows, the load is primarily carried by the solid phase. To determine the conditions under which this is true, we take a closer look at the boundary layer depicted in Fig. 1. First, denote the unknown velocity of the flow at the top of the bed by ΔV. Solving the Darcy-Brinkman equation for $v(y)$, assuming fully developed flow in the x direction, and applying the boundary conditions $v(y = 0) = \Delta V$ (at the top of the bed) and $v(y \to -\infty) \to 0$ (which makes use of the fact that we are operating in a regime where

$\delta/\ell \ll 1$), we find that the flow profile inside the hair bed is given by

$$v(y) = \Delta V\left[\sinh\left(y\sqrt{\frac{\mu}{\mu_e k}}\right) + \cosh\left(y\sqrt{\frac{\mu}{\mu_e k}}\right)\right]. \tag{A1}$$

Just inside the bed at the top interface, the stress in the fluid phase is approximately $\tau_{\text{fluid}} = \mu(\partial v/\partial y)|_{y=0}$, where $v(y)$ is given by Eq. (A1). The portion of the stress carried by the fibers can similarly be estimated as $\tau_{\text{fiber}} = \mu(V - \Delta V)/G$. Hence the ratio of the load carried by the fluid to that carried by the hairs is given by

$$\frac{F_{\text{fluid}}}{F_{\text{hair}}} = \sqrt{\frac{\mu}{\mu_e}}\left(\frac{\Delta V}{V - \Delta V}\right)\frac{G}{\sqrt{k}}\left(\frac{1-\phi_s}{\phi_s}\right). \tag{A2}$$

At this point, we have a reasonable approximation for every quantity in this ratio except ΔV, which can be estimated via force balance on an individual hair.

The three forces acting on each hair are the traction force acting at the tip F_T, the drag force owing to the moving fluid in the boundary layer at the top of the hair bed F_D, and the reaction force anchoring the hair to the substrate F_A. The shear stress acting on the tips of the hairs can be approximated as $\mu(V - \Delta V)/G$; hence the traction force on a single hair is given by $F_T = \mu(V - \Delta V)\pi a^2/G$.

To estimate F_D, we note that the drag per unit length on a single cylinder in a dense periodic array was calculated by Sangani and Acrivos [18] to be

$$f_D(y) = C_0\mu v(y)\left[1 - \left(\frac{\phi_s}{\phi_m}\right)^{1/2}\right]^{-5/2}, \tag{A3}$$

where ϕ_m is the maximum packing fraction of the hairs and C_0 is a dimensionless constant that depends on the structure of the packing; for square arrays $C_0 = 9\pi/2\sqrt{2}$ and for hexagonal arrays $C_0 = 27\pi/4\sqrt{2}$. The total drag force on an individual cylinder can then be computed as $F_D = \int_0^\ell f(y)dy$, yielding

$$F_D = C_0\mu\Delta V\sqrt{\frac{\mu_e k}{\mu}}\left[1 - \left(\frac{\phi_s}{\phi_m}\right)^{1/2}\right]^{-5/2}. \tag{A4}$$

Here k may again be approximated using the expression for the permeability of a dense array of cylinders derived by Gopinath and Mahadevan [8]: $k \approx a^2(1-\phi_s)^2/4\phi_s$.

Finally, the reaction force at the base of the hairs can be estimated by drawing a control volume around the interior of the channel (i.e., the top of the control volume is just inside the top wall of the channel and the bottom of the control volume is just inside the bottom wall of the channel). For this domain, the shear forces acting at the top of the channel must be balanced by the elastic shear stress τ_0 sustained at the base of the fibers (since there is no flow in the bottom portion of the channel), namely, $\mu(V - \Delta V)A/G + \tau_0 A\phi_s = 0$, where A denotes the area of the top and bottom surfaces of the control volume. Solving this force balance for τ_0, we find that the reaction force at the base of an individual fiber is given by $F_A = \tau_0\pi a^2 = -\mu(V - \Delta V)\pi a^2/G\phi_s$.

At equilibrium, $F_T + F_D + F_A = 0$; substituting in the expressions above for each force, applying the Gopinath-Mahadevan approximation for k, and solving for $\Delta V/V$, we find

$$\frac{\Delta V}{V} = \left(1 + \frac{C_0}{2\pi}\frac{G}{a}\sqrt{\frac{\mu_e}{\mu}}\phi_m^{1/2}\psi(\phi_s/\phi_m)\right)^{-1}, \tag{A5}$$

where

$$\psi(\phi_s/\phi_m) \equiv \frac{(\phi_s/\phi_m)^{1/2}}{[1 - (\phi_s/\phi_m)^{1/2}]^{5/2}}. \tag{A6}$$

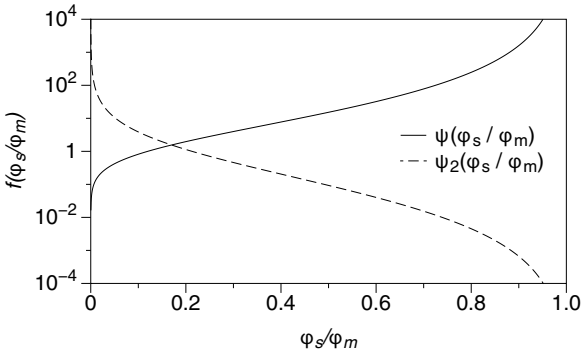

FIG. 6. Functional dependence on ϕ_s/ϕ_m for $\Delta V/V$ and $F_{\text{fluid}}/F_{\text{hair}}$. The solid line depicts $\psi(\phi_s/\phi_m)$ as defined in the text. The dashed line depicts the dependence of $F_{\text{fluid}}/F_{\text{hair}}$ where $\psi_2(\phi_s/\phi_m) \equiv [1 - (\phi_s/\phi_m)^{1/2}]^{5/2}/(\phi_s/\phi_m)$.

Next we note that $C_0/2\pi$, $(\mu_e/\mu)^{1/2}$, and $\phi_m^{1/2}$ are all order one. The ratio of length scales $G/a \approx 10$ in the systems under consideration in this paper. Hence, V is at least an order of magnitude larger than ΔV if $\psi(\phi_s/\phi_m) \gtrsim 1$. Equation (A6) is plotted in Fig. 6, which shows that $\psi(\phi_s/\phi_m) \gtrsim 1$ when $\phi_s/\phi_m \gtrsim 0.1$, a condition that is easily satisfied in the dense limit under consideration.

Finally, we return to Eq. (A2) to address the original question: Under what conditions is the load at the top of the bed carried primarily by the hairs? Combining Eqs. (A2) and (A5), the ratio of the loads carried by the fluid and the hairs simplifies to

$$\frac{F_{\text{fluid}}}{F_{\text{hair}}} \approx \frac{\mu}{\mu_e}\frac{4\pi}{C_0\phi_m}\frac{[1-(\phi_s/\phi_m)^{1/2}]^{5/2}}{\phi_s/\phi_m}. \tag{A7}$$

Given that $\Delta V/V \ll 1$, we have approximated $V - \Delta V \approx V$ and neglected the first term (i.e., the 1) in Eq. (A5). As before, μ/μ_e and $4\pi/C_0\phi_m$ are both order one. Hence, $F_{\text{fluid}} \ll F_{\text{hair}}$ if $[1 - (\phi_s/\phi_m)^{1/2}]^{5/2}/(\phi_s/\phi_m) \ll 1$. This function is shown in Fig. 6, where is it evident that this condition holds provided $\phi_s/\phi_m \gtrsim 0.5$ (a criterion that is easily met in our dense beds). Hence we proceed with the assumption that the bulk of the load at the interface between the hairy region of the channel and the clear region of the channel is carried by the hairs.

[1] O. M. Phillips, J. Fluid Mech. **171**, 563 (1986).
[2] M. A. Koehl, J. R. Koseff, J. P. Crimaldi, M. G. McCay, T. Cooper, M. B. Wiley, and P. A. Moore, Lobster sniffing: Antennule design and hydrodynamic filtering of information in an odor plume, Science **294**, 1948 (2001).
[3] A. Nasto, M. Regli, P.-T. Brun, J. Alvarado, C. Clanet, and A. E. Hosoi, Air entrainment in hairy surfaces, Phys. Rev. Fluids **1**, 033905 (2016).
[4] A. Nasto, P.-T. Brun, and A. E. Hosoi, Viscous entrainment on hairy surfaces, Phys. Rev. Fluids **3**, 024002 (2018).
[5] A. Nasto, P.-T. Brun, and A. E. Hosoi, Drop impact on hairy surfaces, Phys. Rev. Fluids **4**, 064004 (2019).
[6] J. Alvarado, J. Comtet, E. de Langre, and A. E. Hosoi, Nonlinear flow response of soft hair beds, Nat. Phys. **13**, 1014 (2017).
[7] N. Tesla, Valvular conduit, U.S. Patent No. 1,329,559 (3 February 1920).
[8] A. Gopinath and L. Mahadevan, Elastohydrodynamics of wet bristles, carpets and brushes, Proc. R. Soc. A **467**, 1665 (2011).

[9] H. Liu, P. R. Patil, and U. Narusawa, On Darcy-Brinkman equation: Viscous flow between two parallel plates packed with regular square arrays of cylinders, Entropy **9**, 118 (2007).
[10] M. A. R. Koehl, How do benthic organisms withstand moving water? Am. Zool. **24**, 57 (1984).
[11] S. Vogel, Drag and flexibility in sessile organisms, Am. Zool. **24**, 37 (1984).
[12] S. Vogel, Drag and reconfiguration of broad leaves in high winds, J. Exp. Bot. **40**, 941 (1989).
[13] F. F. Erian, S. Corrsin, and S. H. Davis, Maternal, placental blood flow: A model with velocity-dependent permeability, J. Biomech. **10**, 807 (1977).
[14] L. Landau and B. Levich, Dragging of a liquid by a moving plate, Acta Physicochimica U.R.S.S. **17**, 42 (1942).
[15] B. Derjaguin, On the thickness of the liquid film adhering to the walls of a vessel after emptying, Acta Physicochim. U.R.S.S. **20**, 349 (1943).
[16] H. Jeffreys, The draining of a vertical plate, Math. Proc. Cambridge **26**, 204 (1930).
[17] A. M. Nasto, Hairy interfaces, Ph.D. thesis, Massachusetts Institute of Technology, 2018.
[18] A. S. Sangani and A. Acrivos, Slow flow part periodic arrays of cylinders with application to heat transfer, Int. J. Multiphase Flow **8**, 193 (1982).